Article

A Study on Functional Hydrophobic Stainless Steel 316L Using Single-Step Anodization and a Self-Assembled Monolayer Coating to Improve Corrosion Resistance

Chanyoung Jeong

Department of Advanced Materials Engineering, Dong-Eui University, 176 Eomgwang-ro, Busanjin-gu, Busan 47340, Korea; cjeong@deu.ac.kr; Tel.: +82-51-890-2286; Fax: +82-505-182-6898

Abstract: Stainless steel fabricated using chromium is widely being used in various industries due to its superior corrosion resistance compared to light metals such as aluminum, titanium, and magnesium. However, despite its excellent properties, a problem of poor corrosion resistance in harsh environments remains. In this study, an economical and environmentally friendly anodizing process was applied to the surface of stainless steel (SUS 316L) to create porous nanostructures to improve its water-repellent properties. In these experiments, voltages of 30, 50, 70, and 90 V were applied to stainless steel for 3 h to form an oxide film, prior to immersion in 0.1 M phosphoric acid for 10 min to expand the oxide pores. In addition, the change of the oxide structure was observed through field-emission scanning electron microscopy (FE-SEM). In terms of the contact angle, hydrophilicity was observed at applied voltages of 70 and 90 V, in which a porous film was formed; the best water repellency was observed at a 90 V applied voltage, after the application of an FDTS (1H,1H,2H,2H-perfluorodecyltrichlorosilane) coating, a self-assembled monolayer. Finally, the corrosion behavior of a hydrophobic specimen was tested using potentiodynamic polarization (PDP) experiments. The hydrophobic SUS 316L alloy subsequently displayed improved corrosion resistance in a 3.5 wt% NaCl solution.

Keywords: stainless steel; anodizing; oxide film; hydrophobic coating; corrosion resistance

1. Introduction

Studies of hydrophobic surfaces are being currently being conducted in attempts to improve the corrosion resistance of metals and their alloys [1]. Specifically, research into the improvement of corrosion resistance of stainless steel is gaining attention [2]. Due to inherent features such as corrosion resistance, economic feasibility, and machinability, stainless steel that contains chrome is being widely used in industries including machinery, electronic component production, maritime engineering, power generation, nuclear power generation, and piping [3]. However, stainless steel has a tendency to lose its resistance due to pitting and different forms of corrosion in the piping and maritime industries, especially where the environment is notably harsh [4].

A common method to prevent corrosion is to use surface treatment methods comprising various metals [5], which can involve electrochemical, mechanical, and chemical methods. One of the more popular methods of prevention is to improve water repellency by controlling the wetting behavior [6]. Wettability occurs due to the thermodynamic equilibrium between the solid, liquid, and gaseous states when a droplet of water is added onto a solid surface. This process can be digitized by using the contact angle, and the water repellency can then be obtained when the contact angle between the surface and water is over 90° [7]. Surfaces having a high level of water repellency express anticorrosion [8], antifreezing [9], self-cleaning [10], and antistaining properties, all of which are required in various industries [11].

Importantly, the wetting behavior can be affected by the energy of the material surface [12]. This means that the lower the value of the surface energy, the greater the water repellency; i.e., the higher the value, the more hydrophilic the surface. These characteristics are determined by the nano- and micro-sized structures of the surface [13,14]. Methods used to prevent the generation of these structures on the surface include the application of a chemical conversion coating, as well as plasma electrolytic oxidation [15]. However, these methods are generally unable to meet today's industrial requirements, either because they are not economically feasible or due to the fact that they can cause severe environmental pollution [16].

In contrast, anodization methods—electrochemical methods—have been studied because, in addition to the fact that the nano- and micro-sized structures can be controlled [17], they include advantages such as economic feasibility and environmental friendliness [18]. Anodization methods are now being used to produce a thick and even oxide film on the metallic substrate of the test sample [19], as the process involves submerging the metal test sample in a liquid electrolyte and then connecting the metal test sample to the positive electrode and coupling the auxiliary electrode to the negative electrode [20,21]. After the anodization process is prepared and the power is supplied, oxygen is produced and an oxide film is formed on the metal substrate due to the production of oxygen [22]. The size and shape of the nanostructures on the oxide film produced during the anodization process can subsequently be controlled by adjusting the electrolyte, voltage, time, stirring speed, and temperature [23].

This oxide film can be further divided into a barrier-type film with no voids, because of the dense structure of the film, and a porous-type film having multiple pore structures in a pattern [24]. Controlling the voltage of the oxide film on the surface of stainless steel is of particular importance, as trivalent chrome forms chrome oxide (Cr_2O_3) on the surface of the stainless steel in a trivalent state (Figure 1a) [25]. However, because the chrome ions in a hexavalent state are highly soluble in an aqueous solution, the oxide film on the stainless steel will dissolve in the acid electrolyte when the applied potential is higher than the chrome production potential [26]. Therefore, voltage control is seen to be an important factor in the production of oxide films on the surface of stainless steel.
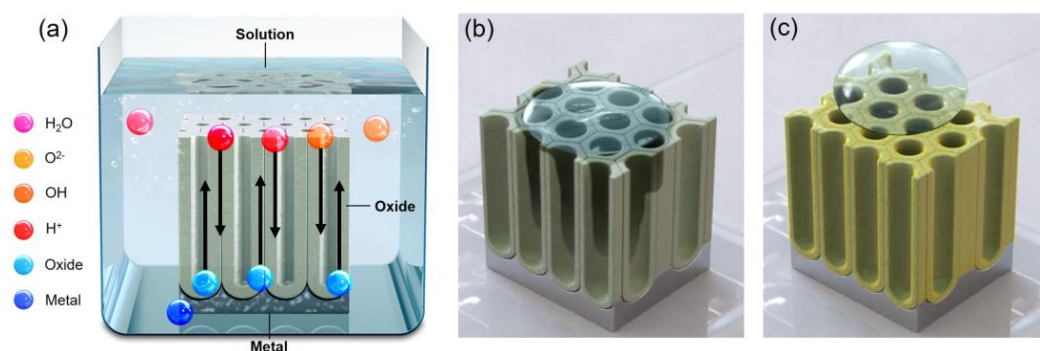

Figure 1. Schematics of (**a**) the creation of a nano-oxide structure using an anodizing method in solution, (**b**) the hydrophilic (wetted) property on a nano-oxide surface, and (**c**) the hydrophobic (dewetted) property on a nano-oxide surface.

SUS 316L stainless steel is the material of interest for this paper because it is commonly used in industries since it contains molybdenum and features a higher level of corrosion resistance than other standard types of stainless steel such as SUS 304 [27]. However, an insufficient number of studies have been conducted on improving its level of corrosion resistance and water repellency for the purpose of preventing pitting corrosion and other types of corrosion. Since the surface structure plays an important role in maximizing the level of water repellency, the pores of multiporous nanostructures on the surface of the stainless steel samples are widened by using an anodization method (Figure 1b) [28]. Next, water repellency is achieved by applying a thin layer of 1H,1H,2H,2H-perfluorodecyltrichlorosilane (FDTS), a material having a low level of surface energy, to the nanostructures that are

essentially hydrophilic because of their low level of solid fraction [29]. This way, there will be layers of oxide, water-repellent coating, and oxygen on the surface of the stainless steel [30], improving its resistance to pitting corrosion in comparison to bare stainless steel whose surface is not treated (Figure 1c) [31].

2. Materials and Methods

Stainless steel (SUS 316L) was cut into 3 cm × 3 cm × 0.05 cm squares to be used in the tests, and its chemical composition is shown in Table 1 [32]. To clean the surface, the test sample was submerged in an ultrasonic cleaner, first with ethanol and then with acetone, for 10 min in each, before drying. For the anodization process, platinum (2.5 cm × 4 cm × 0.05 cm) was used as the negative electrode, and stainless steel was used as the positive electrode. The distance between the two electrodes was maintained at 5 cm throughout the anodization process. A solution containing ethylene glycol ($C_2H_6O_2$; Junsei Chemical Co., Ltd., Tokyo City, Japan), 0.1 M of distillate, and 0.1 M of ammonium fluoride (NH_4F; Junsei Chemical Co., Ltd., Tokyo City, Japan) was used as the electrolyte, which was maintained at 0 °C using a water-cooled chiller and jacketed beaker in order to prevent deterioration of the test piece.

Table 1. Chemical composition of stainless steel 316L [32].

	C	Mn	P	S	Ni	Cr	Mo	Fe
SUS 316L	0.03	2.00	0.45	0.03	12.0–15.0	16.0–18.0	2.0–3.0	Bal.

The anodization voltage was increased from 30 V to 50, 70, and 90 V, and each voltage was applied to the test sample for a total of 3 h. The test piece was then cleaned with distillate and dried after anodization. The test piece was subsequently submerged in 0.1 M of phosphoric acid (H_3PO_4, Junsei Chemical Co., Ltd., Tokyo City, Japan) for a total of 10 min in order to expand the nanostructures produced during the anodization process. The piece was then coated with a self-assembled monolayer by using FDTS, a material with a low level of surface energy, in order to add water repellency to the surface of the test piece, which has now gone through the anodization and pore widening process [33].

Next, as a precoating process, the surface of the test sample was treated with oxygen plasma to remove any remaining organic residue and was then heat-treated at a temperature of 150 °C for a total of 10 min. Field-emission scanning electron microscopy (FE-SEM) and EDS were used in the structural analysis and observation of the structural form of the oxide film on the surface of the stainless steel applied during the anodization process. To evaluate the wettability, approximately 3.0 μL of water was injected onto the test sample at room temperature by using a contact angle analyzer. The tests for each sample were repeated more than five times. A potentiodynamic polarization (PDP) test was then conducted in order to observe the corrosion behavior. The test sample was measured after submerging it in a 3.5 wt% NaCl solution. The test was conducted using a three-electrode system, with the test sample used as the working electrode, platinum (Pt) as the counter electrode, and silver/silver chloride (Ag/AgCl) as the reference electrode. In terms of measurement conditions, the sample was measured five times per test condition, at a speed of 1 mV/s in the range of −500 to +14,000 mV (vs. Ag/AgCl).

3. Results and Discussion

3.1. Fabrication Stainless Steel Anodizing

Figure 2 and Table 2 show the results of the test sample component analysis that was obtained using EDS, before and after anodization. Compared to the untreated test sample, the anodized test sample has a higher level of oxygen content, due to the production of an oxide film, in which chrome, molybdenum, nickel, manganese, and phosphorus were detected. Figure 2 and Table 2 show that an oxide film is produced on the surface of the anodized test sample. Figure 3 shows the SEM images of the test sample surface at each applied voltage, after 3 h of testing. Figure 3a–d shows the top view images at 30, 50, 70,

and 90 V, respectively. The images show that unlike the surface of Figure 3c,d, a barrier-type oxide film is formed on the surface of Figure 3a,b and that no pores are formed on the surface. However, the images show that, unlike the former samples, multiporous structures are formed on the samples shown in Figure 3c,d. The reason for the formation of these multiporous structures is that the level of roughness of the oxide film surface increased due to the partial dissolution of the film surface when the oxide film was exposed to the acidic solution.
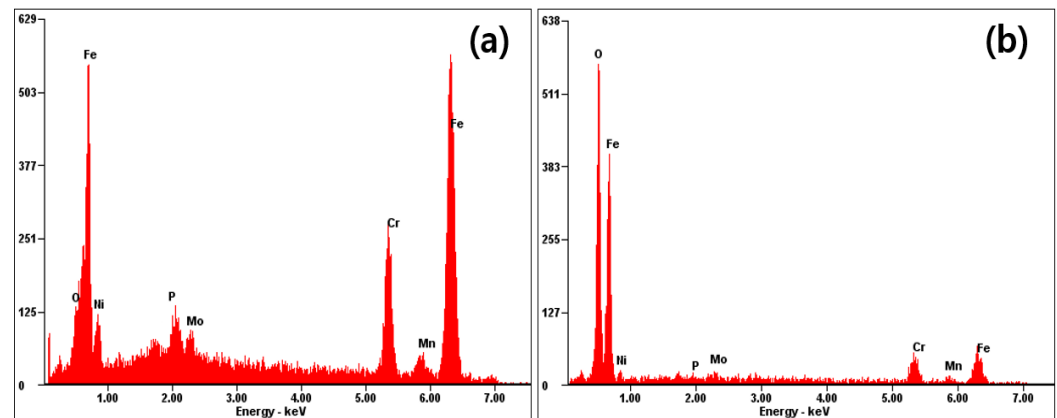

Figure 2. EDS analyses used to compare before and after anodization: (**a**) stainless steel 316L and (**b**) stainless steel 316L after anodization at 90 V.

Table 2. EDS analysis data of bare stainless steel and anodized stainless steel 316L.

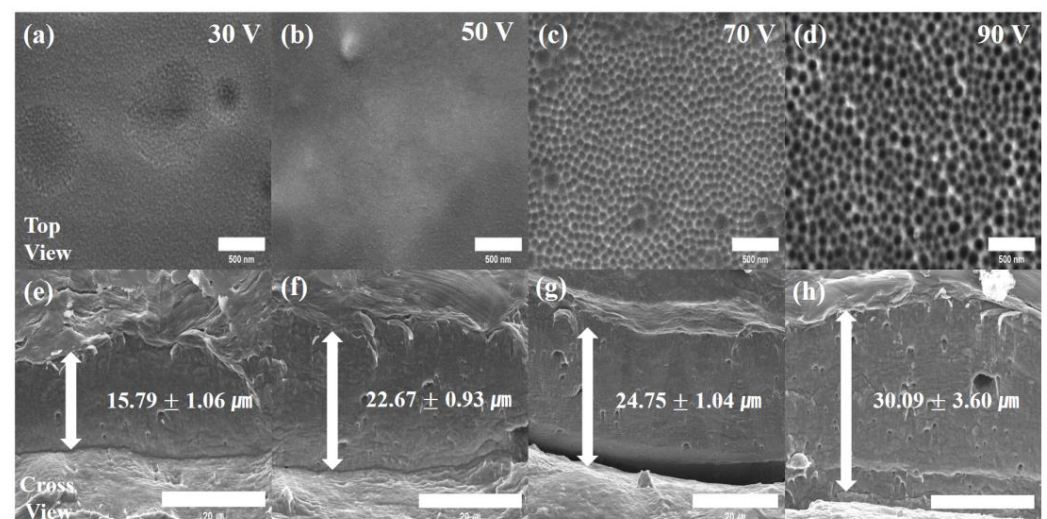| Sample	Elements (at%)						
	O	**Ni**	**P**	**Mo**	**Cr**	**Mn**	**Fe**
SUS 316L	10.87	11.99	2.83	1.54	16.25	3.17	53.35
SUS 316L Anodized	75.17	2.62	0.16	0.81	7.12	1.41	12.71

Figure 3. SEM images of oxide films on the surface after anodization for each voltage, at a treatment time of 3 h: top view at (**a**) 30 V, (**b**) 50 V, (**c**) 70 V, and (**d**) 90 V (scale bar: 500 nm); cross view at (**e**) 30 V, (**f**) 50 V, (**g**) 70 V, and (**h**) 90 V (scale bar: 20 μm).

Figure 3e–h shows the thickness of the anodized film by voltage. As the voltage increased from 30 V to 50, 70, and 90 V, the anodized film thickness increased. The film

appears to become thicker as more positive ions are produced as the voltage is increased, accelerating the oxidation [34].

The SEM images shown in Figure 3 were used to obtain the pore diameter (DP), interpore distance (D_{int}), and the solid fraction values (Table 3). The pore diameter and interpore distance were obtained as an average value, and the solid fraction was calculated using Equation (1) [35,36].

$$f_{SL} = 1 - \frac{2\pi}{\sqrt{3}} \left(\frac{r}{a} \right)^2 \tag{1}$$

where 'f_{SL}' is the solid fraction, 'a' is the interpore distance, and 'r' is the pore diameter. No pores were found in the barrier-type oxide films of the samples having applied voltages of 30 and 50 V, so the D_P, D_{int}, and solid fraction values could not be obtained. However, the D_P, D_{int}, and solid fraction values could be calculated for samples applied with voltages of 70 and 90 V, as multiple pores were produced. At 70 V, the D_P, D_{int}, and solid fraction values were 68.62 ± 8.07 nm, 89.78 ± 8.30 nm, and 0.4559, respectively. At 90 V, the calculated values were 92.17 ± 8.25 nm, 106.45 ± 7.22 nm, and 0.3201.

Table 3. Characterization of the oxide film structure of stainless steel 316L.

	D_P (nm)	D_{int} (nm)	Solid Fraction
30 V	Not available	Not available	Not available
50 V	Not available	Not available	Not available
70 V	68.62 ± 8.07	89.78 ± 8.30	0.4559
90 V	92.17 ± 8.25	106.45 ± 7.22	0.3201

3.2. Characterization of Wettability

The contact angle after anodization for each voltage is shown in Figure 4. The angle is 57.4° ± 5.36° at 30 V, 36.7° ± 1.59° at 50 V, 24.3° ± 4.36° at 70 V, and 13.2° ± 0.60° at 90 V, confirming the degree of hydrophilicity. The higher the applied voltage, the lower the contact angle observed.
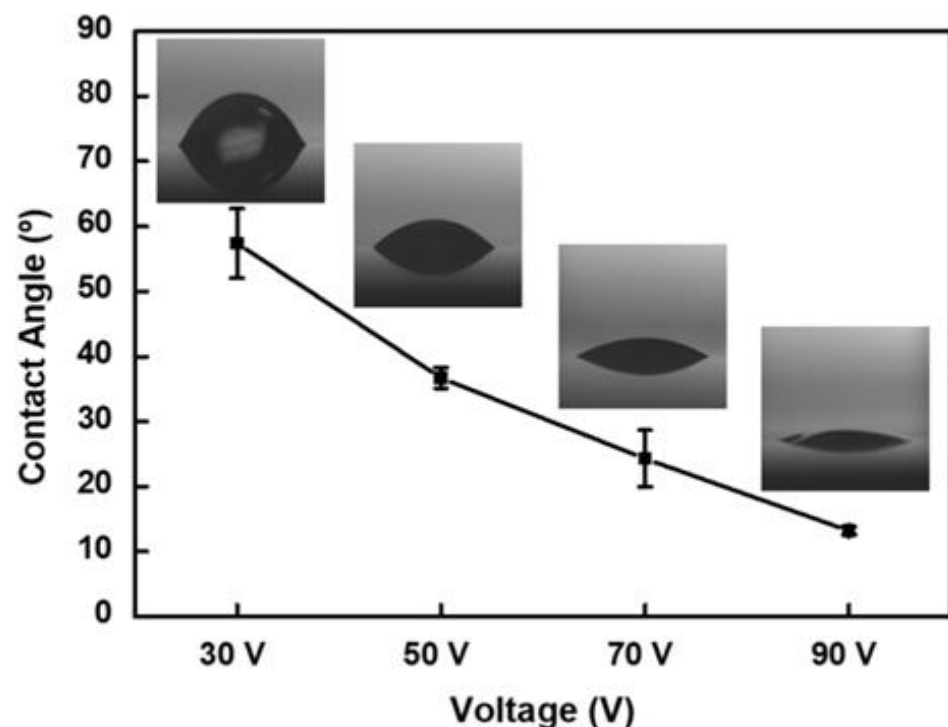

Figure 4. Contact angles before FDTS was coated on the anodized stainless steel 316L samples, at applied voltages of 30, 50, 70, and 90 V.

Figure 5 shows the contact angle after self-assembled monolayer coating is applied by using FDTS at a low surface energy level in the nanostructures produced during the anodization process. The angle is $115.5° \pm 2.58°$ at an applied voltage of 30 V, $123.4° \pm 1.63°$ at 50 V, $133.4° \pm 1.82°$ at 70 V, and $141.4° \pm 1.37°$ at 90 V. These results confirm that the higher the applied voltage, the higher the contact angle.
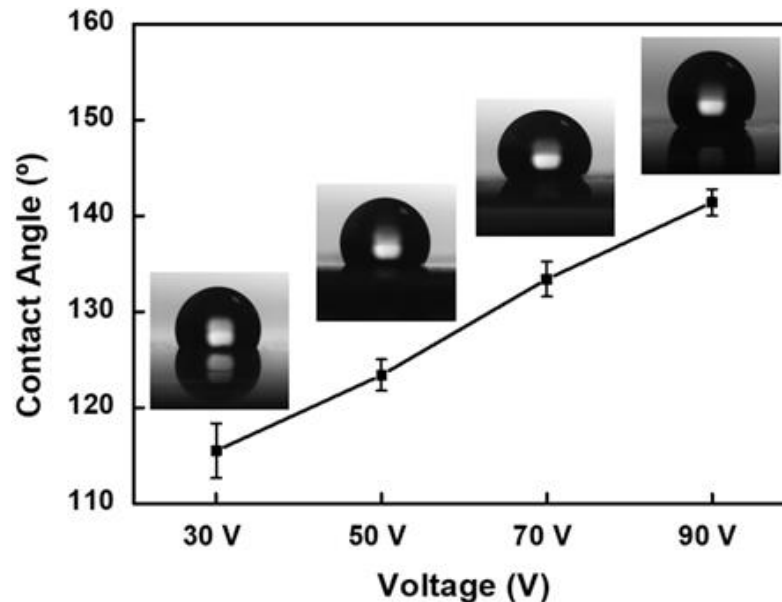

Figure 5. Contact angle after FDTS is coated on the anodized stainless steel 316L sample, at applied voltages of 30, 50, 70, and 90 V.

In accordance with the Cassie–Baxter equation, air pushes out the water droplets on the pores or solid surfaces of a multiporous oxide film, so it is determined that the contact angle is higher on a multiporous test sample surface that is coated. The contact angles in Figures 4 and 5 are summarized in Table 4 [37].

Table 4. Contact angle between anodized stainless steel and FDTS coated stainless steel 316L according to the applied voltage.

	Anodization	Anodization + Coating
30 V	$57.4° \pm 5.36°$	$115.5° \pm 2.85°$
50 V	$36.7° \pm 1.59°$	$123.4° \pm 1.63°$
70 V	$24.3° \pm 4.36°$	$133.4° \pm 1.82°$
90 V	$13.2° \pm 0.60°$	$141.4° \pm 1.37°$

3.3. Analysis of Potentiodynamic Polarization

Figure 6 shows the results of the PDP tests for the bare SUS 316L and FDTS-coated hydrophobic oxide films with different oxide parameters such as pore diameter and interpore distance and oxide thicknesses in 3.5 wt% NaCl solution after immersion for 1 h. The E_{corr}, I_{corr}, and IE values for the samples are also summarized in Table 5. The corrosion potential refers to the potential that is generated on the test sample surface that corrodes due to the standard electrode in an open circuit condition. From these results, corrosion tends to occur faster because there is a higher oxidation tendency when the value is lower [38]. In terms of the corrosion current density, more current flows when the current density value is higher, so more corrosion tends to occur. In addition, the inhibition efficiency is calculated in numbers by using the corrosion current density; 'i' is the current density of the anodized and coated test sample, and 'i_0' is expressed as the current density of the untreated test sample, obtained using Equation (2).

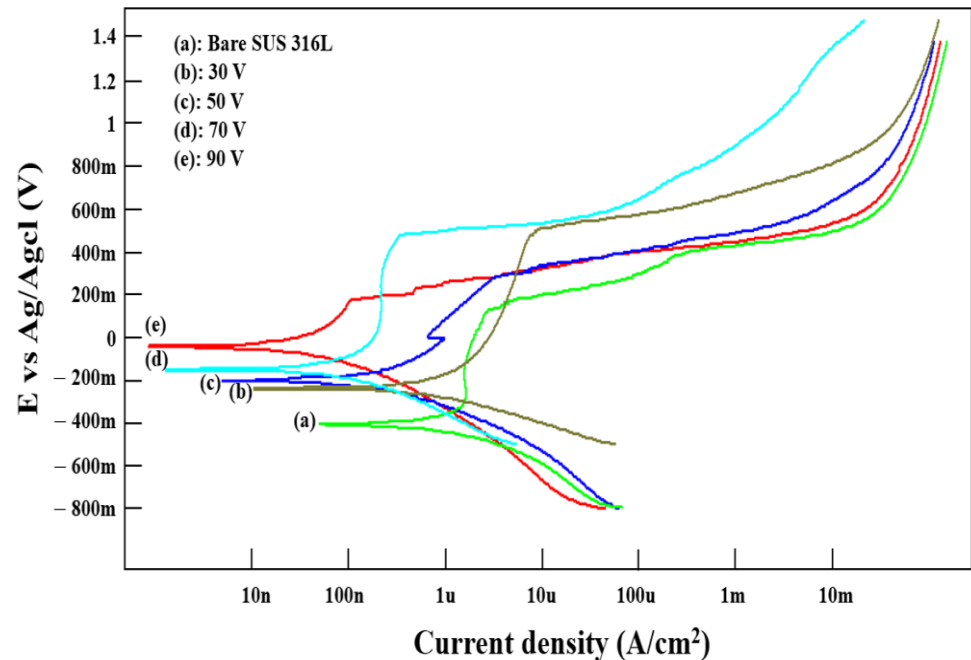$$IE\% = \left(1 - \frac{i}{i_0}\right) \times 100 \tag{2}$$

Figure 6. PDP test result of bare SUS 316L and 316L of FDTS-coated stainless steel anodized according to each applied voltage.

Table 5. PDP test values of bare SUS 316L and anodized stainless steel 316L with FDTS coating according to the applied voltage.

Samples	E_{corr} (mV)	I_{corr} (A/cm^2)	IE (%)
SUS 316L	-404.2 ± 5.84	$2.36 \pm 0.13 \times 10^{-7}$	0
30 V anodized	-232.2 ± 3.18	$1.67 \pm 0.2 \times 10^{-7}$	29.23
50 V anodized	-192.4 ± 3.61	$1.16 \pm 0.17 \times 10^{-7}$	50.84
70 V anodized	-144.6 ± 1.62	$2.49 \pm 0.12 \times 10^{-8}$	89.44
90 V anodized	-38.3 ± 4.61	$9.02 \pm 0.36 \times 10^{-9}$	96.18

The E_{corr} of the untreated test sample (SUS 316L) is -404.2 ± 5.84 mV, and the I_{corr} is $2.36 \pm 0.13 \times 10^{-7}$ A/cm^2. These values are -232.2 ± 3.18 mV and $1.67 \pm 0.2 \times 10^{-7}$ A/cm^2 when the applied voltage with FDTS coating is 30 V, -192.4 ± 3.61 mV and $1.16 \pm 0.17 \times 10^{-7}$ A/cm^2 at 50 V, -144.6 ± 1.62 mV and $2.49 \pm 0.12 \times 10^{-8}$ A/cm^2 at 70 V, and -38.3 ± 4.61 mV and $9.02 \pm 0.36 \times 10^{-9}$ A/cm^2 at 90 V, respectively. The E_{corr} was inclined to shift in a positive direction with the increase in the oxide thickness, which was more pronounced with a larger pore diameter and interpore distance. The I_{corr} was decreased with the increase in pore diameter, which was more pronounced in the thicker oxide film. The result that I_{corr} decreases with the increase in pore diameter and thickness suggest that the impregnated air layer is more efficient than bare SUS 316L and thin oxide layer in protecting the surface from corrosion. The estimated IE values of the FDTS-coated SUS 316L anodized samples are 29.23% at 30 V, 50.84% at 50 V, 89.44% at 70 V, and 96.18% at 90 V, showing the improved corrosion resistance with the increase in oxide parameters, pore diameter, thickness, and air fraction. The 90 V sample with the largest pore diameter, the greatest thickness, and the smallest solid fraction shows the best IE value, which means the larger air fraction in terms of both the surface area and the volume. Thus, the tendency is that the higher the applied voltage conditions, the higher the corrosion resistance level.

These results correspond to the changes in the surface structure of the material and the wettability of the water-repellent treated multiporous oxide film when in contact with a corrosive material (Cl^-). In the case of changes in the surface structure of materials that come into contact with corrosive substances, coated materials that have a low level of surface energy do not have electrodes, making it difficult for water molecules to attach to their surface, and also for corrosive substances in the water molecules to produce chemical reactions on the coated metal. In accordance with the Cassie–Baxter state, it is determined that it is also difficult for corrosive substances to penetrate into the pores, due to air filling the pores when the multiporous oxide film is water-repellent treated, thereby improving its corrosion prevention potential [39,40].

4. Conclusions

In this paper, the SUS 316L surface was improved using an anodization technique and FDTS coating for anticorrosion. Observations of the form of the anodized film obtained by changing the applied voltage show that a thin film is formed at an applied voltage of 30 and 50 V, while a porous oxide film is formed at 70 and 90 V. In addition, it can be confirmed that pores are large when the applied voltage is 70 V or higher. This has a superhydrophilic effect as the solid fraction value on the surface decreases. That is, the correlation between the solid fraction and the hydrophilicity could be confirmed by calculating the solid fraction value according to the state of each oxide film. As described above, FDTS, a material with a low energy level, was coated on the superhydrophilic surface with a low solid fraction to realize a superhydrophobic (ultra-water-repellent) surface with a contact angle of 140 degrees or more. It was shown that the hydrophobicity of the anodized film obtained at voltages of 70 and 90 V by Cassie equations was the highest. The reason for this is that there is air in the oxide pores, so the water repellency is maintained. Corrosion behavior was observed in each of the hydrophobic SUS 316L samples treated by both anodizing and coating methods. It was shown that the corrosion value was excellent as the water repellency increased. Accordingly, the SUS 316L sample has a superhydrophilic property under the condition of the applied 90 V anodizing voltage. When FDTS coating was applied here, it had superhydrophobic property, and the best corrosion prevention efficiency could be confirmed. It is believed that this is because thick oxides film as insulating layers, and at the same time, the air is present in the oxide pores, thereby maintaining the hydrophobic property and making it difficult for Cl ions, which are external factors, to penetrate. Therefore, the results indicate the FDTS-coated superhydrophobic oxide film with a larger pore diameter and a greater oxide film thickness is more efficient at preventing corrosion, with a resistance value as high as over 96%, because of a minimized solid fraction which means a greater capability of the air within the pores to repel the corrosive medium from touching the bottom metal surface. As a result, it is expected that the corrosion resistance of SUS 316L stainless steel will be further improved to prevent the product from being easily corroded, especially in harsh environments, thereby confirming positive economic benefits. Significant economic and environmental effects can be expected by applying this type of waterproof stainless steel surface to various industrial fields.

Institutional Review Board Statement: Not applicable.

Informed Consent Statement: Not applicable.

Data Availability Statement: Not applicable.

Conflicts of Interest: The author declares no conflict of interest.

References

1.　Cai, Y.; Chang, W.; Luo, X.; Sousa, A.M.; Lau, K.H.A.; Qin, Y. Superhydrophobic structures on 316L stainless steel surfaces machined by nanosecond pulsed laser. *Precis. Eng.* **2018**, *52*, 266–275. [CrossRef]

2.　Klimas, V.; Pakstas, V.; Vrublevsky, I.; Chernyakova, K.; Jagminas, A. Fabrication and Characterization of Anodic Films onto the Type-304 Stainless Steel in Glycerol Electrolyte. *J. Phys. Chem. C* **2013**, *117*, 20730–20737. [CrossRef]

3.　Lee, C.; Kim, J. Surface Modification Method of Stainless Steel using Electrochemical Etching. *J. Korean Soc. Precis. Eng.* **2014**, *31*, 353–358. [CrossRef]

4.　Metroke, T.L.; Parkhill, R.L.; Knobbe, E.T. Passivation of metal alloys using sol–gel-derived materials—A review. *Prog. Org. Coat.* **2001**, *41*, 233–238. [CrossRef]

5.　Zhilei, C.; Maobing, S.; Lida, W. Cathodic etching for fabrication of super-hydrophobic aluminum coating with micro/nano-hierarchical structure. *J. Solid State Electrochem.* **2013**, *17*, 2661–2669. [CrossRef]

6.　Feng, L.; Che, Y.; Liu, Y.; Qiang, X.; Wang, Y. Fabrication of superhydrophobic aluminium alloy surface with excellent corrosion resistance by a facile and environment-friendly method. *Appl. Surf. Sci.* **2013**, *283*, 367–374. [CrossRef]

7.　Vazirinasab, E.; Jafari, R.; Momen, G. Application of superhydrophobic coatings as a corrosion barrier: A review. *Surf. Coat. Technol.* **2018**, *341*, 40–56. [CrossRef]

8.　Zhang, F.; Zhao, L.; Chen, H.; Xu, S.; Evans, D.G.; Duan, X. Corrosion Resistance of Superhydrophobic Layered Double Hydroxide Films on Aluminum. *Angew. Chem.* **2008**, *120*, 2500–2503. [CrossRef]

9.　Cao, L.; Jones, A.K.; Sikka, V.K.; Wu, J.; Gao, D. Anti-icing superhydrophobic coatings. *Langmuir* **2009**, *25*, 12444–12448. [CrossRef]

10.　Sarshar, M.A.; Swarctz, C.; Hunter., S.; Simpson., J.; Choi., C.-H. Self-cleaning surfaces—Virtual realities. *Nat. Mater.* **2003**, *2*, 301–306.

11.　Lim, H.E.; Park, J.S.; Kim, W.D. Micro/nanostructured Superhydrophobic Surface. *Elastomers Compos.* **2009**, *44*, 244.

12.　Kalin, M.; Polajnar, M.J.T.I. The correlation between the surface energy, the contact angle and the spreading parameter, and their relevance for the wetting behaviour of DLC with lubricating oils. *Tribol. Int.* **2013**, *66*, 225–233. [CrossRef]

13.　Song, D.; Lian, B.; Fu, Y.; Wang, G.; Qiao, Y.; Klu, E.E.; Gong, X.; Jiang, J. Dual-Layer Corrosion-Resistant Conversion Coatings on Mg-9Li Alloy via Hydrothermal Synthesis in Deionized Water. *Metals* **2021**, *11*, 1396. [CrossRef]

14.　Jeong, C.; Choi, C.H. Single-step direct fabrication of pillar-on-pore hybrid nanostructures in anodizing aluminum for superior superhydrophobic efficiency. *ACS Appl. Mater. Interfaces* **2012**, *4*, 842–848. [CrossRef] [PubMed]

15.　Yerokhin, A.L.; Snizhko, L.O.; Gurevina, N.L.; Leyland, A.; Pilkington, A.; Matthews, A. Discharge characterization in plasma electrolytic oxidation of aluminium. *Appl. Phys.* **2003**, *36*, 2110. [CrossRef]

16.　Wang, Z.; Li, Q.; She, Z.; Chen, F.; Li, L. Low-cost and large-scale fabrication method for an environmentally-friendly superhy-drophobic coating on magnesium alloy. *J. Mater. Chem.* **2012**, *22*, 4097. [CrossRef]

17.　Boinovich, L.B.; Emelyanenko, A.M.; Modestov, A.D.; Domantovsky, A.G.; Emelyanenko, K.A. Synergistic Effect of Superhy-drophobicity and Oxidized Layers on Corrosion Resistance of Aluminum Alloy Surface Textured by Nanosecond Laser Treatment. *ACS Appl. Mater. Interfaces* **2015**, *7*, 19500–19508. [CrossRef] [PubMed]

18.　Xu, Q.F.; Wang, J.N.; Sanderson, K.D. A general approach for superhydrophobic coating with strong adhesion strength. *J. Mater. Chem.* **2010**, *20*, 5961. [CrossRef]

19.　Lee, W.; Nielsch, K.; Gösele, U. Self-ordering behavior of nanoporous anodic aluminum oxide (AAO) in malonic acid anodization. *Nanotechnology* **2007**, *18*, 8. [CrossRef]

20.　Lee, W.; Ji, R.; Gösele, U.; Nielsch, K. Fast fabrication of long-range ordered porous alumina membranes by hard anodization. *Nat. Mater.* **2006**, *5*, 741–747. [CrossRef]

21.　Lee, W.; Scholz, R.; Gösele, U. A continuous process for structurally well-defined Al$_2$O$_3$ nanotubes based on pulse anodization of aluminum. *Nano Lett.* **2008**, *8*, 2155–2160. [CrossRef] [PubMed]

22.　Nosonovsky, M.; Bhushan, B. Biomimetic superhydrophobic surfaces: Multiscale approach. *Nano Lett.* **2007**, *7*, 2633–2637. [CrossRef] [PubMed]

23.　Chen, Y.; Zhang, Y.; Shi, L.; Li, J.; Xin, Y.; Yang, T.; Guo, Z. Transparent superhydrophobic/superhydrophilic coatings for self-cleaning and anti-fogging. *Appl. Phys. Lett.* **2012**, *101*, 033701. [CrossRef]

24.　Jeong, C. Nano-Engineering of Superhydrophobic Aluminum Surfaces for Anti-Corrosion. Ph.D. Thesis, Stevens Institute of Technology, Hoboken, NJ, USA, 2013.

25.　Hassan, A.; Ali, G.; Park, Y.J.; Hussain, A.; Cho, S.O. Formation of a self-organized nanoporous structure with open-top morphology on 304L austenitic stainless steel. *Nanotechnology* **2020**, *31*, 315603. [CrossRef] [PubMed]

26.　Ji, H.; Jeong, C. Fabrication of Superhydrophobic Aluminum Alloy Surface with Hierarchical Pore Nanostructure for Anti-Corrosion. *Corros. Sci. Technol.* **2019**, *18*, 228.

27.　Jeong, C.; Ji, H. Systematic Control of Anodic Aluminum Oxide Nanostructures for Enhancing the Superhydrophobicity of 5052 Aluminum Alloy. *Materials* **2019**, *12*, 3231. [CrossRef] [PubMed]

28.　Wang, Z.; Paschalidou, E.; Seyeux, A.; Zanna, S.; Maurice, V.; Marcus, P. Mechanisms of Cr and Mo Enrichments in the Passive Oxide Film on 316L Austenitic Stainless Steel. *Front. Mater.* **2019**, *6*, 232. [CrossRef]

29.　Park, E.J.; Cho, Y.K.; Kim, D.H.; Jeong, M.G.; Kim, Y.H.; Kim, Y.D. Hydrophobic polydimethylsiloxane (PDMS) coating of mesoporous silica and its use as a preconcentrating agent of gas analytes. *Langmuir* **2014**, *30*, 10256–10262. [CrossRef]

30. Jeong, C.; Lee, J.; Sheppard, K.; Choi, C.H. Air-Impregnated Nanoporous Anodic Aluminum Oxide Layers for Enhancing the Corrosion Resistance of Aluminum. *Langmuir* **2015**, *31*, 11040–11050. [CrossRef]
31. Hu, P.; Xie, Q.; Ma, C.; Zhang, G. Silicone-Based Fouling-Release Coatings for Marine Antifouling. *Langmuir* **2020**, *36*, 2170–2183. [CrossRef]
32. Wang, H.; Shuro, I.; Umemoto, M.; Ho-Hung, K.; Todaka, Y. Annealing behavior of nano-crystalline austenitic SUS316L produced by HPT. *Mater. Sci. Eng. A* **2012**, *556*, 906–910. [CrossRef]
33. Cai, Q.; Paulose, M.; Varghese, O.K.; Grimes, C.A. The Effect of Electrolyte Composition on the Fabrication of Self-Organized Titanium Oxide Nanotube Arrays by Anodic Oxidation. *J. Mater. Res.* **2005**, *20*, 230–236. [CrossRef]
34. Jani, A.M.; Losic, D.; Voelcker, N.H. Nanoporous anodic aluminium oxide: Advances in surface engineering and emerging applications. *Prog. Mater. Sci.* **2013**, *58*, 636–704. [CrossRef]
35. Park, Y.; Jeong, C. Study on a Superhydrophobic Stainless Steel (SUS 304) Surface to Enhance Corrosion Resistance. *Korean J. Met. Mater.* **2021**, *59*, 217–222. [CrossRef]
36. Kim, S.H.; Jeong, C. Feasibility of Machine Learning Algorithms for Predicting the Deformation of Anodic Titanium Films by Modulating Anodization Processes. *Materials* **2021**, *14*, 1089. [CrossRef] [PubMed]
37. Cassie, A.; Baxter, S. Wettability of porous surfaces. *Trans. Faraday Soc.* **1944**, *40*, 546. [CrossRef]
38. Jeong, C.; Choi, C.H. Google Patents. 2014. Available online: http://google.com/patent/US20140255682A1/en (accessed on 11 September 2014).
39. Lee, W. The anodization of aluminum for nanotechnology applications. *JOM* **2010**, *62*, 57–63. [CrossRef]
40. Song, H.; Kim, M.; Jung, G.; Vang, M.; Park, Y. The effects of spark anodizing treatment of pure titanium metals and titanium alloys on corrosion characteristics. *Surf. Coat. Technol.* **2007**, *201*, 8738–8745. [CrossRef]